ARMY RESEARCH LABORATORY

AR

The Performance and Deformation Behavior of Oriented Columnar-Grained Tungsten Polycrystalline Penetrators

by Lee S. Magness, Wendy A. Leonard, Deepak Kapoor, Moon Chung, and Jeffrey Trogolo

ARL-TR-1666   May 1998

Army Research Laboratory
Aberdeen Proving Ground, MD 21005-5066

The Performance and Deformation Behavior of Oriented Columnar-Grained Tungsten Polycrystalline Penetrators

Lee S. Magness, Wendy A. Leonard
Weapons and Materials Research Directorate, ARL

Deepak Kapoor, Moon Chung
U.S. Army Armament Research, Development, and Engineering Center

Jeffrey Trogolo
Niche Microstructural Corporation

Abstract

The flow and failure of monocrystalline tungsten penetrators, during the penetration of armor targets, has been shown to be anisotropic. The penetration performances of the single crystal penetrators were found to be a function of the crystallographic orientation of the penetrator axis. The performance of the [100]-oriented tungsten penetrators was roughly equivalent to that of depleted uranium penetrators.

In this series of ballistic experiments, the performance and deformation behaviors of polycrystalline tungsten penetrators having oriented columnar grains in [100], [110], or [111] directions were examined.

Acknowledgments

The authors would like the acknowledge the following people who have contributed to this project.

INTENTIONALLY LEFT BLANK.

Table of Contents

List of Figures

List of Tables

INTENTIONALLY LEFT BLANK.

1. Introduction

High-density materials, primarily uranium alloys or tungsten-based metal matrix composites, are used as penetrator cores in modern kinetic energy (KE) projectiles. In this application, uranium projectiles have been shown to offer superior penetration performance. However, concerns about the environmental and occupational hazards associated with the manufacture, deployment, and use of the uranium rounds prompt efforts to develop a tungsten-based material that will equal or surpass the ballistic performance of uranium alloys.

For many years, increases in the ballistic performance of tungsten-based composites (WBC) (i.e., tungsten heavy alloys [WHA]) were sought through improving the mechanical properties of the penetrator material. However, despite successes in significantly increasing the strengths and toughnesses of WHAs, the basic penetration performances of these alloys did not improve (Leonard, Magness, and Kapoor 1992). It is now well documented that the flow and failure behaviors of the penetrator material, not the values of strength or ductility measured in a conventional mechanical test, are the most important determiners of penetration performance. The flow-softening and shear localization behavior of the uranium-3/4% titanium (U-3/4% Ti) alloy has been shown to be responsible for the greater penetration performance of these projectiles (Magness and Farrand 1990).

Bruchey, Horwath, and Kingman (1990, 1991) demonstrated that anisotropies in the flow and failure of monocrystalline tungsten penetrators can also influence ballistic performance. The ballistic performance of a monocrystalline tungsten penetrator depended on whether the penetrator axis was oriented along the [100], [110], or [111] direction in the crystal. Penetrators with the [100] axis oriented parallel to the penetrator axis performed much better than conventional WHAs, achieving penetration depths close to that of uranium alloy penetrators. Tungsten monocrystal penetrators with a [111] orientation penetrated to depths comparable to those of conventional WHAs, while monocrystal penetrators with a [110] orientation did not perform as well as the conventional WHAs.

1

While these results showed that [100]-oriented tungsten single-crystal penetrators could offer penetration performances comparable to that of uranium alloys, there are a number of practical difficulties with their use as penetrator core materials. A major problem is the brittleness of the single crystals, which are prone to cleavage failures along {100} planes. They would therefore be difficult to launch from a cannon and would certainly be poor performers against spaced plate or other complex armor designs. Another practical issue is the potentially high cost of manufacturing large tungsten single crystals.

Possible alternatives to the tungsten monocrystals might be a heavily textured polycrystalline tungsten, with the tungsten grains oriented by mechanical working or thermomechanical processing, or a WHA composite, with a strong preferred orientation of the tungsten particle component. As a first step in this direction, this study examined whether melt-grown columnar grain tungsten penetrators would exhibit the distinct, orientation-dependent deformation behaviors and ballistic performances seen for the single-crystal penetrators. With large columnar grains strongly oriented in the [100], [110], or [111] directions, the degree of crystallographic orientation of these materials is far superior to that possible in either a textured tungsten phase or in an oriented tungsten phase WHA. The qualities of the grain orientations in each material were characterized by means of electron backscattered diffraction (EBSD) and x-ray diffraction. After ballistic testing, the residual penetrators were sectioned and examined metallographically to compare the flow and failure mechanisms for each orientation.

2. Characterization of Oriented Columnar-Grained Tungsten Polycrystals

2.1 Processing History. The columnar-grained tungsten samples used in this study were procured from the former Soviet Union, under Contract No. DAAL-04-94-M-S260. Bar stock, 17 mm in diameter and in lengths ranging from 400 to 600 mm (Figure 1), were drawn from a melt in a plasma-arc furnace. By using seed crystals with the specific starting orientations, the bars were produced with the columnar grains oriented in the [100], [110], and [111] directions.
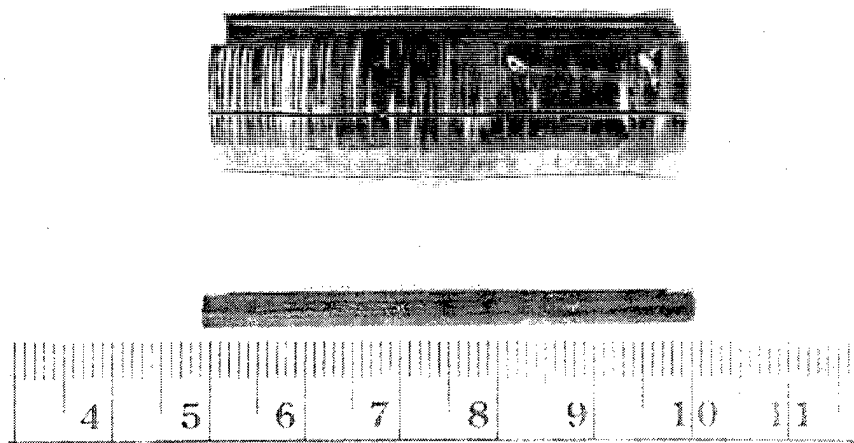
Figure 1. Photograph of Original Bar Stock and a Subscale Penetrator.

Both quarter-scale and subscale penetrators were cut from the bar stock. Due to the brittleness of the columnar-grained materials, conventional machining was not possible and the penetrators had to be electrical-discharge-machined (EDM). In all cases, the axes of the penetrators were aligned parallel to the axis of each bar. Prior to ballistic testing, samples of the materials were first examined using optical metallography, x-ray diffraction analysis (Leonard et al. 1995), and EBSD analysis (Trogolo 1995) to assess the quality of the crystallographic orientations of the grains.

2.2 Optical Metallography. Typical examples of the microstructures observed in the metallographic examinations are shown in Figures 2 and 3. The columnar-grained structure is evident in the longitudinal and transverse cross sections of the bar stock. In the etched transverse cross section (Figure 3), the individual grain boundaries can be identified as sharp lines. The patterns of etch pits inside these boundaries delineate the boundaries of the numerous subgrains within the individual grains. Individual grain sizes varied from 0.1 to 1 mm, and subgrains from 100 to 300 μm across in the transverse sections. Subsequent EBSD and x-ray diffraction studies verified that the columnar grains in the melt-grown tungsten bar stock were strongly oriented in the respective [100], [110], or [111] directions.
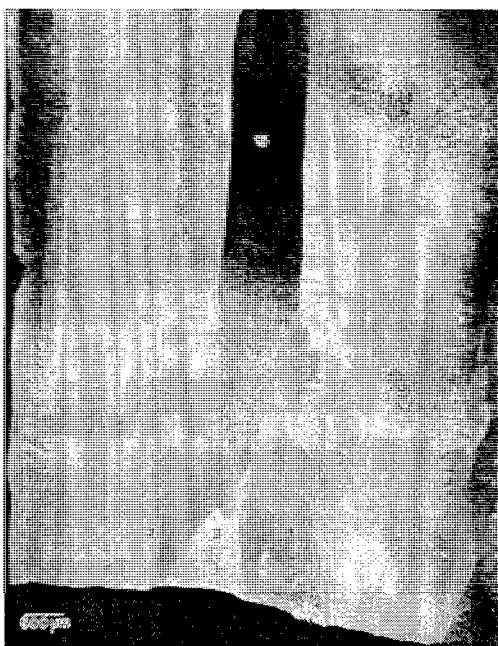
Figure 2. Micrograph of Longitudinal Section.
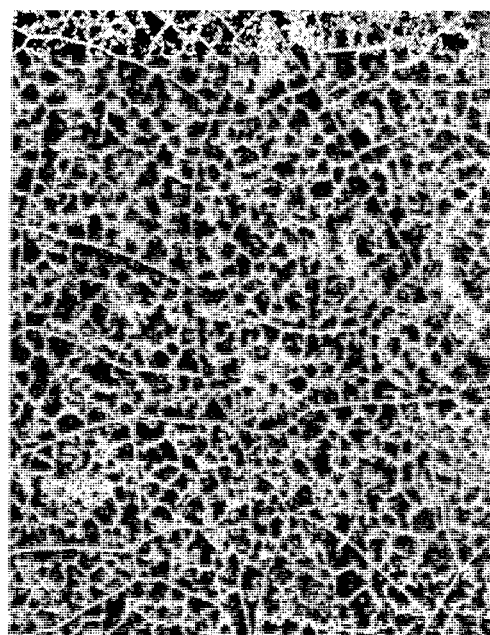
Figure 3. Micrograph of Transverse Section.

2.3 X-ray Diffraction Analysis. Samples of each orientation were sent to the Metallic Materials Branch at Picatinny Arsenal. The surfaces perpendicular to the original axis of the bar stock (penetrator) were examined by x-ray diffraction. The specimens were first analyzed with a Siemens D5000 x-ray diffractometer, using Cu Kα radiation at 40 kV and 30 mA. The diffraction scans confirmed that an extremely high concentration of (100), (110), or (111) planes lay parallel to the specimen surface for samples having [100], [110], or [111] growth orientations, respectively (Figure 4). X-ray texture analysis was subsequently applied to each of the specimens, using the Siemens D5000 diffractometer with a Huber cradle attachment and Mo Kα radiation at 50 kV and 30 mA. The texture analysis verified that the specimens had the highly textured structure expected of an oriented columnar-grained structure or directionally solidified crystal.

2.4 EBSD Analysis. Similar samples of the bars were examined by EBSD analysis at Niche Microstructural Corporation. EBSD analysis utilizes backscattered electrons, those in the incident

4
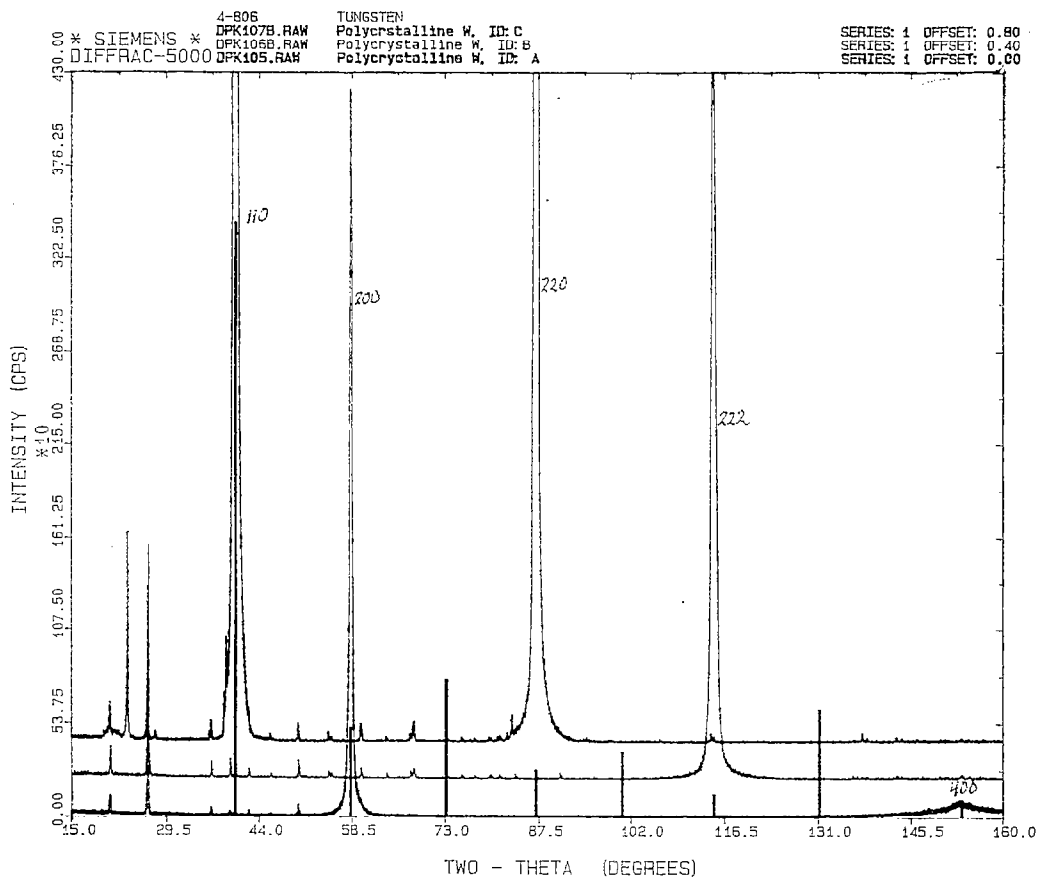
Figure 4. Results of the X-ray Diffraction Scans.

beam of a scanning electron microscope (SEM) that are diffracted by the crystal planes in a specimen, to produce a pattern of intersecting bands. The pattern produced is analogous to the Kikuchi patterns observed in transmission electron microscopy (TEM). Since the angular relationships between the planes in the crystal are preserved in the bands of the EBSD pattern, the analysis of the pattern can be used to determine the crystallographic orientation of the individual grains and, in turn, their relationship with each of their neighbors. With a spatial resolution of ~0.5 μm and an angular resolution of ~0.5°, EBSD is applicable to fine microstructures and sensitive to subtle misorientations.

EBSD analysis characterizes a grain aggregate through two primary measurements. The first measurement, grain orientation, is the orientation of the crystal with respect to the specimen

5

reference frame. The information about the orientations of the grains allows one to determine the loading (resolved shear stresses) on the various slip planes. The second measurement, grain (or boundary) misorientation, is the crystal orientation at one point (on one side of a grain boundary) relative to that at another point (on the opposite side of the boundary). This angle determines the structure of the boundaries between the grains that will interact with the moving dislocations. Both of these microstructural characteristics are expected to influence the response of the columnar grain tungsten materials under the high-rate deformation (back extrusion) of the penetrator core during the ballistic impact.

Samples of tungsten specimens having growth directions [100], [110], and [111] were analyzed using EBSD. Grain orientation was measured by ϕ, the angle between the crystal growth direction and the specimen axis (see Figure 5). In Figures 6a–c, the distribution of these grain orientations for each of the three specimens are plotted. Bimodal distributions of orientations were found in the [100] and [111] samples (Figures 6a and c). This indicates that the bars contained two sets of grains, with an angle of misalignment with respect to the growth direction (specimen axis) of about 2.6° and 1.4°, respectively. In both cases, the peak at the higher angle is less than the peak at the lower angle. This variation could be due to either the widespread occurrence of two orientation variations, or to two separate regions of different alignment within the specimen. The [110] sample, by contrast, had a narrower, and not bimodal, distribution of grain orientations (Figure 6b).

The grain or boundary misorientation of two adjacent grains can be related by a single rotation through which the two crystal lattices become coincident. This rotation is described by a particular misorientation axis (*uvw*) and an angle of rotation (θ) about that axis to bring the crystals into coincidence (Figure 7). The position of the misorientation axis can be measured by α, the angle between the misorientation axis and the specimen growth axis. If $\alpha = 0°$, the relationship between the two measured crystals is pure tilt (Figure 8a). If $\alpha = 90°$, the relationship is pure twist (Figure 8c). The distribution of these angles provides some insight into the misorientation trends of the substructure.
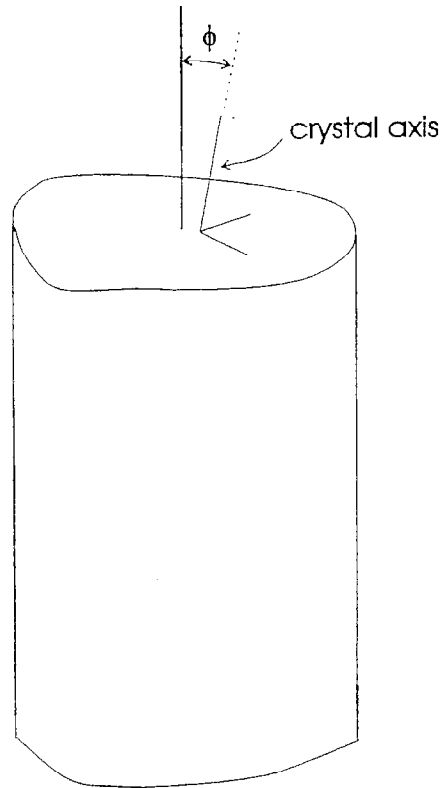
Figure 5. Measurement of Grain Orientation Angle, ϕ.

The distributions of grain boundary misorientations are depicted by the histograms of the angle of rotation or misorientation angle, θ, in Figures 9 and 10. The θ distribution indicates that the majority of rotations are very low; however, some are over $5°$. These higher values are important because, in some applications, a material's behavior is often limited by the extreme, not the average, values.

The distribution of α in Figure 10 shows a broad range of axis orientations. However, superimposed on the general distributions are small concentrations ($\sim 10\%$) at particular angles from the growth directions ($\alpha \sim 45°$, $30°$, and $35°$ for [100], [110], and [111] orientations, respectively). These concentrations, or peaks, in the distributions suggest the presence of a preferred boundary misorientation, or mesotexture.

In summary, the EBSD crystallographic analysis of [100]-, [110]-, and [111]-oriented tungsten determined that there is a small but measurable range of grain orientations in these columnar
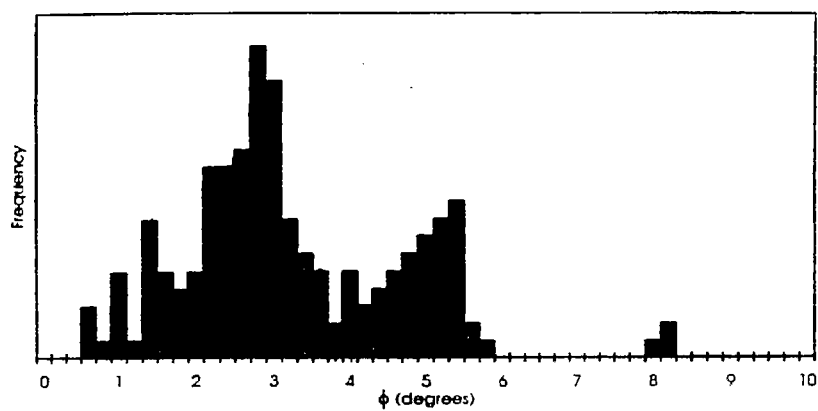
(a) [100] Orientation.
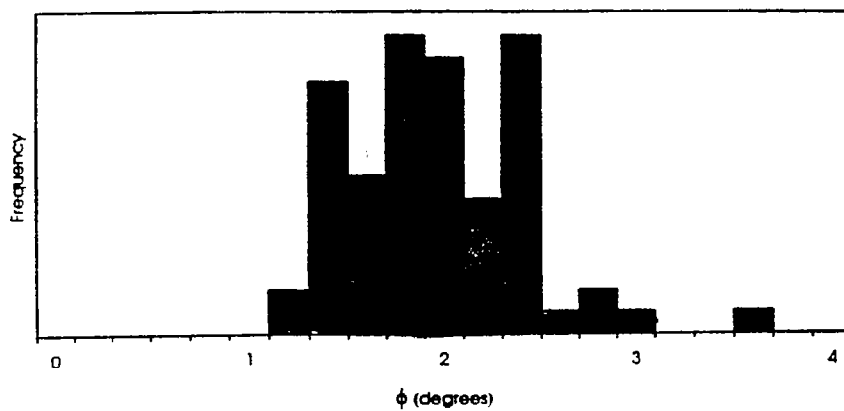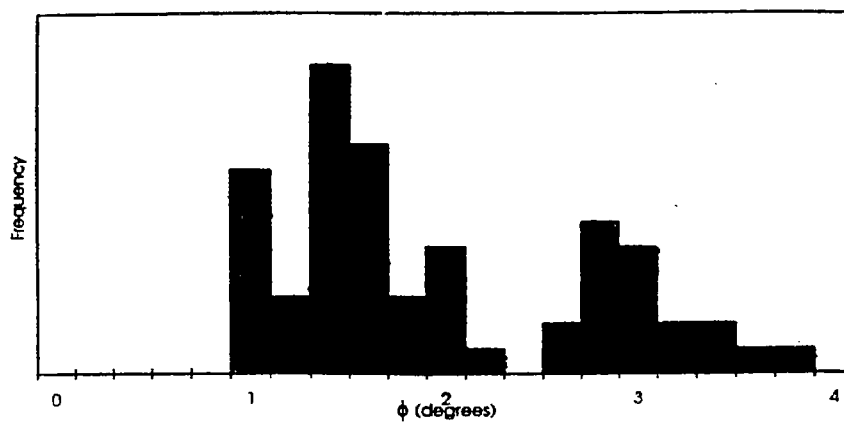
(b) [110] Orientation.

(c) [111] Orientation.

Figure 6. Distribution of Grain Orientations, φ, Between Crystal Growth Direction and Specimen Axis.

8
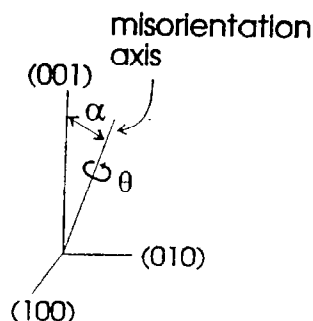
Figure 7. Boundary Misorientation Measurement Notation.

(a)   (b)   (c)
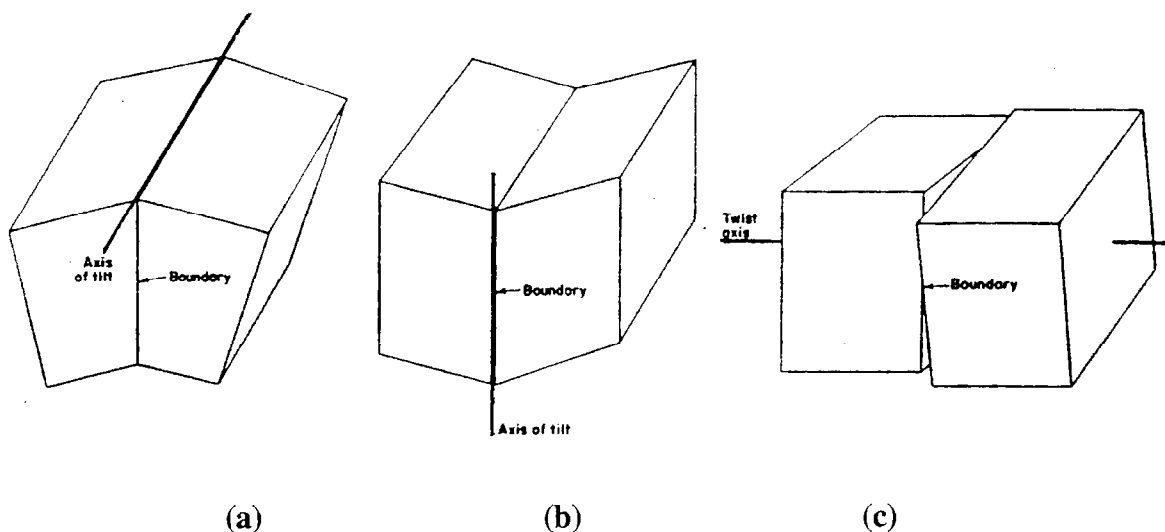
Figure 8. Grain Boundary Degrees of Freedom.

microstructures. The misorientation between adjacent grains was found to be generally small; however, there are a significant number of misorientations larger than a few degrees. The low-angle boundaries associated with these misorientations will probably influence the high-strain-rate deformation behavior exhibited during ballistic impact by interacting with the rapidly moving dislocations.

3. Ballistic Testing Procedures and Results

Penetrators were cut from the bar stock by EDM, with the axes of the penetrators aligned parallel to the axis of each bar. Sufficient bar stock was available for the [100] orientation, the most

9
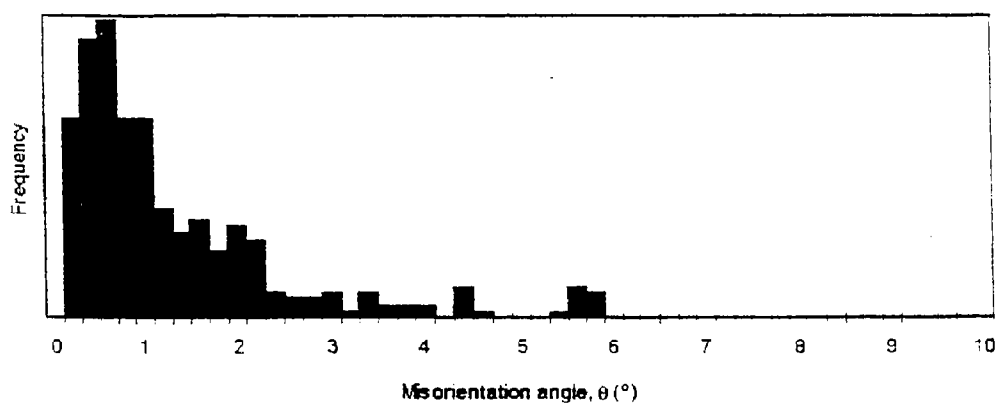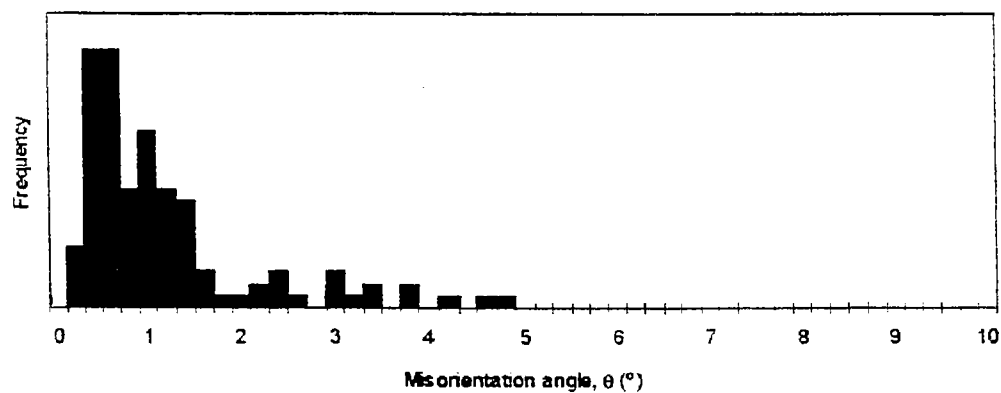
(a) [100] Orientation.
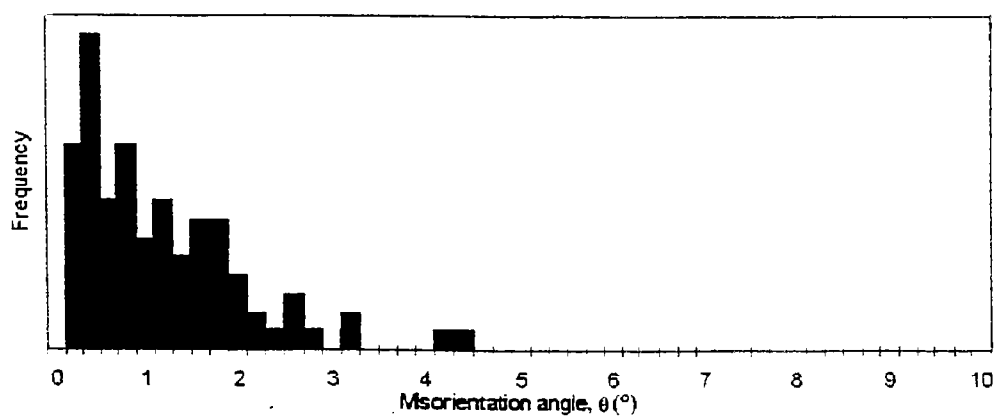
(b) [110] Orientation.

(c) [111] Orientation.

Figure 9. Distribution of Misorientation Angle, θ, Between Adjacent Subgrains.

10
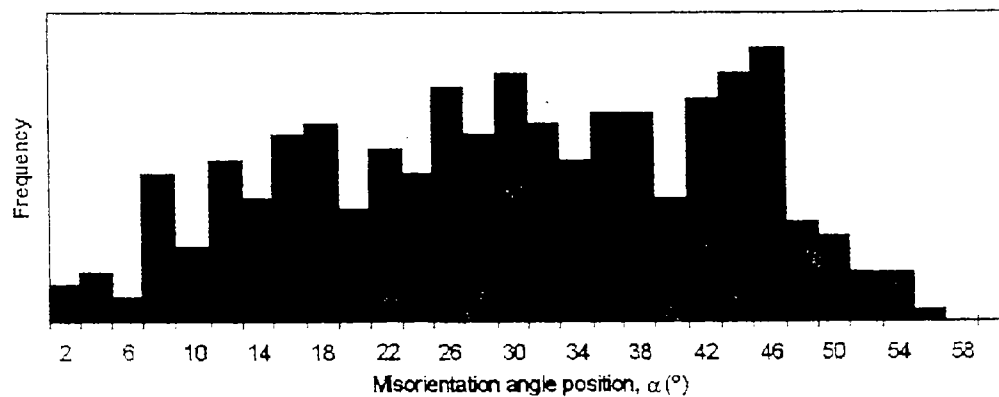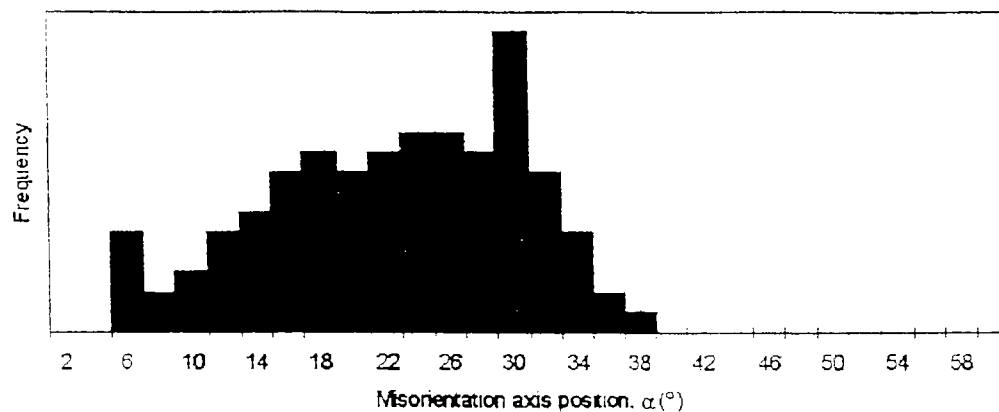
(a) [100] Orientation.
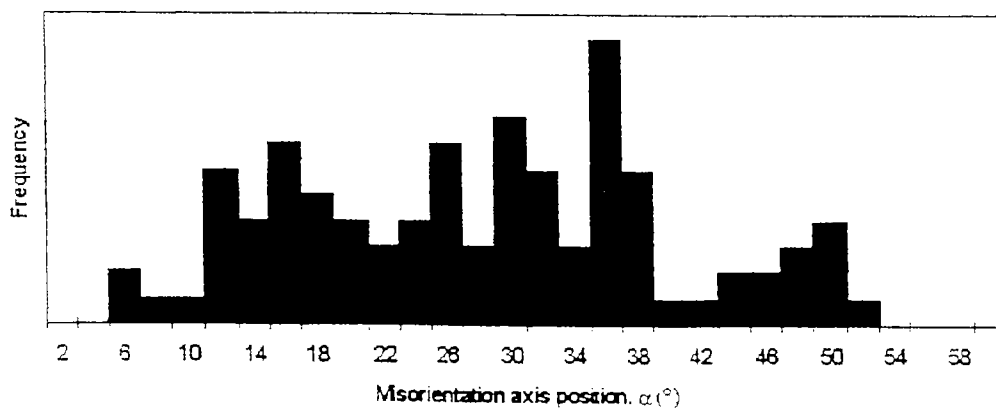
(b) [110] Orientation.

(c) [111] Orientation.

Figure 10. Distribution of α, the Angle Between the Growth Axis and the Misorientation Axis Between Adjacent Subgrains.

11

promising orientation in the monocrystal tests, to machine both quarter-scale and subscale penetrators. For the other two orientations, only subscale penetrators could be tested.

Quarter-scale penetrators, with a mass of 65 g, were cut to length-to-diameter (L/D) ratios of 10. The rods have diameters that are 7.59 mm (0.299 in) and lengths of 75.9 mm (2.99 in). The subscale penetrators are 3.81 mm (0.15 in) in diameter by 50.8 mm (2.0 in) in length (L/D of 13.33) and have an approximate mass of 11 g. Six subscale penetrators could be machined out of the cross section of the original bar stock.

Due to brittleness of the columnar-grained tungsten (in all three orientations), the penetrators proved to be difficult to test, generally shattering under the acceleration loads occurring during their launch from the laboratory gun. A reverse ballistic technique, in which the target was launched at a stationary penetrator, was therefore used to assess penetration performance. In this test setup, the penetrator was mounted on a lightweight fixture in front of a 50-mm smoothbore gun and the "target," a mild steel cylinder with a length of 50.8 mm (2.0 in) and a diameter of 46.99 mm (1.85 in), was launched at the stationary penetrator. The target was captured in a soft-catch recovery pack, consisting of 52 1-in plywood squares, behind the penetrator-target impact location. A steel washer was placed a few millimeters behind the rear of the penetrator. The impact of the washer would close or seal the entrance to the penetration cavity, preventing the residual penetrator from being dislodged from the target during the subsequent deceleration of the cylinder in the soft-catch recovery pack. A photograph of the penetrator fixture is shown in Figure 11.

After each test, the recovered target was sectioned to measure the depth of penetration and to reveal the embedded residual penetrator. The soft recovery technique placed a limit on the velocity and energy of the target that could be safely captured by the pack. Almost all of the subscale reverse ballistic tests were conducted at a velocity near 1,015 m/s.

The penetration performances of each of the three columnar-grained orientations are summarized in Table 1. For comparison, identical geometry, subscale penetrators of U-3/4% Ti, conventional 93- and 97-weight-percent tungsten WHAs, and polycrystalline unalloyed tungsten with fine,
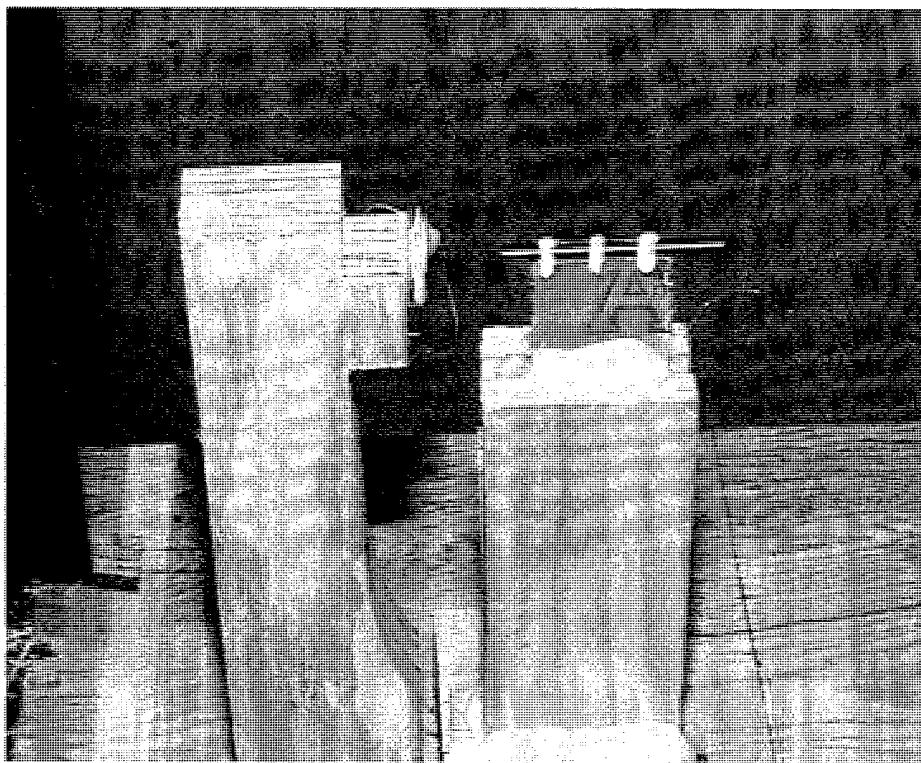
Figure 11. Photograph of Reverse Ballistic "Penetrator" Fixture.

random-oriented grains (nonsag tungsten) were also tested. The depths of penetration were adjusted for slight deviations from the desired impact velocity of 1,015 m/s.

The same data are presented graphically in Figure 12. Since these materials have different densities, each of these identical geometry penetrators have different masses. Penetration, therefore, is plotted as a function of penetrator mass in Figure 12. The complete data set, collected from all of the tests, is listed in the appendix.

Albeit a much weaker dependence than observed by Bruchey, Horwath, and Kingman (1990) for the monocrystal penetrators, the penetration performances of these oriented columnar-grained tungsten penetrators also appear to be a function of their crystallographic orientation. There is a significant amount of scatter in the penetration data presented in Table 1 and Figure 12, but the relative rankings of the orientations were identical to those found previously for the monocrystal

13

Table 1. Reverse Ballistic Penetration Data Adjusted to a 1,015-m/s Impact Velocity

Material	Density (g/cm³)	Mass (g)	Adjusted Penetration (mm)
93% W	17.6	10.3	26.0
93% W	17.6	10.3	27.0
97% W	18.6	10.77	27.7
97% W	18.6	11.14	27.7
97% W	18.6	10.99	28.8
Nonsag W	19.3	11.38	27.0
[100]	19.3	11.34	30.3
[100]	19.3	11.46	31.2
[100]	19.3	11.39	29.3
[100]	19.3	10.82	28.3
[110]	19.3	10.96	24.5
[110]	19.3	11.35	26.2
[111]	19.3	11.28	25.0
[111]	19.3	11.46	29.8
U-3/4% Ti	19.3	10.93	38.9
U-3/4% Ti	19.3	11.0	40.6
U-3/4% Ti	19.3	10.9	39.9

NOTE: W = tungsten.

penetrators (section 5). The magnitudes of the differences in penetration depths between each of the orientations, however, were much smaller than reported for the monocrystal penetrators.

As in the tests of the monocrystal penetrators, the performances of the [110] columnar-grained tungsten, on average, were the worst, and the performances of the [100] columnar-grained material were better than those of the [110] and [111] orientations, of the random-orientation, fine-grain,
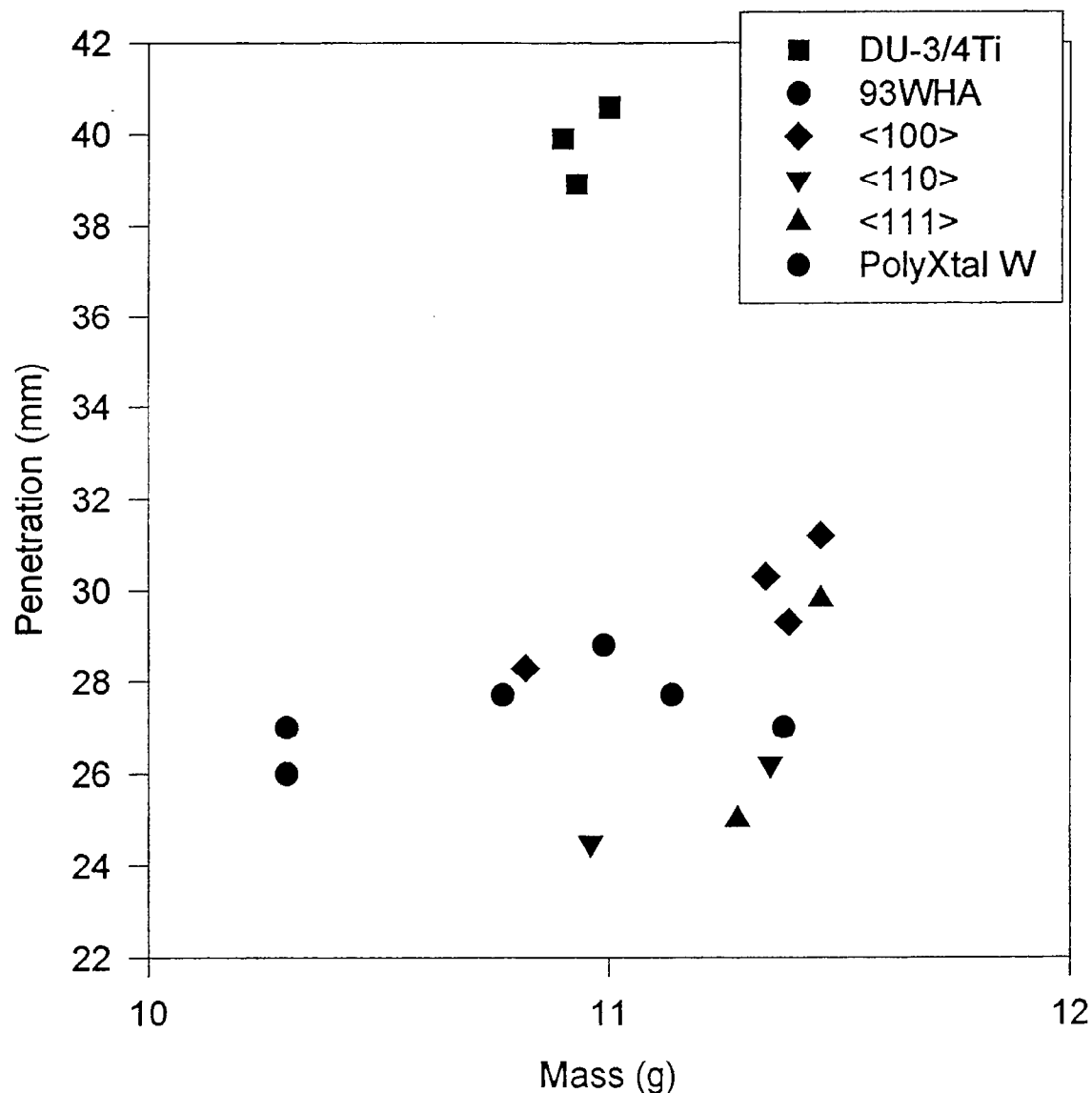
Figure 12. Penetration Depth as a Function of Penetrator Mass (Subscale Tests, Constant 1,015-m/s Impact Velocity).

nonsag tungsten rod, and of the conventional WHA penetrators. However, the penetrations achieved by all of the columnar-grained orientations fell short of those of the U-3/4% Ti alloy rods.

As mentioned earlier, the columnar-grained tungsten penetrators proved to be too brittle to survive launch in a normal, forward ballistic test. A number of the quarter-scale columnar tungsten penetrators were saboted and fired from the laboratory cannon. All of them fractured in bore during launch, and no useful penetration data could be collected. To overcome this brittle fracture problem,

two [100]-oriented columnar tungsten rods were jacketed in steel, using a plasma-spraying process developed by Materials Resources, Inc. (Kim, Smith, and Kapoor 1996). For comparison, side-by-side tests were conducted using conventional WHA penetrators with the same overall dimensions and approximately the same aggregate density. The low-density steel jacket on the [100]-oriented columnar-grained rods reduced the aggregate density of the penetrators to slightly less than that of a 90-weight-percent tungsten content WHA. The penetration depths achieved by the jacketed [100] orientation penetrators and two 90-weight-percent tungsten WHA penetrators are tabulated in Table 2 and presented graphically in Figure 13.

Table 2. Quarter-Scale Ballistic Results

Penetrator Material	Mass_{pen} (g)	$V_{striking}$ (m/s)	Yaw (°)	Penetration (mm)
[100] with steel jacket	46.05	1,187	0.25	43
[100] with steel jacket	44.52	1,294	1.27	50
90.7% WHA	49.71	1,186	1.27	40
90.7% WHA	49.83	1,294	0.56	48

These larger scale tests were consistent with the results of the subscale tests. Despite slightly lower penetrator masses, the jacketed [100]-oriented columnar-grained penetrators offered slightly greater penetration performances than the conventional WHA penetrators having the same dimensions.

4. Metallographic Observations of Flow and Failure Behaviors

The residual columnar-grained tungsten polycrystalline penetrators, embedded in the mild steel target cylinders, were examined metallographically. The sectioned targets were polished and examined at the tungsten processing facility at Picatinny Arsenal, Dover, NJ, and by Murr and Pappu (1997) at the University of Texas, El Paso. In section 5, the flow and failure behaviors of
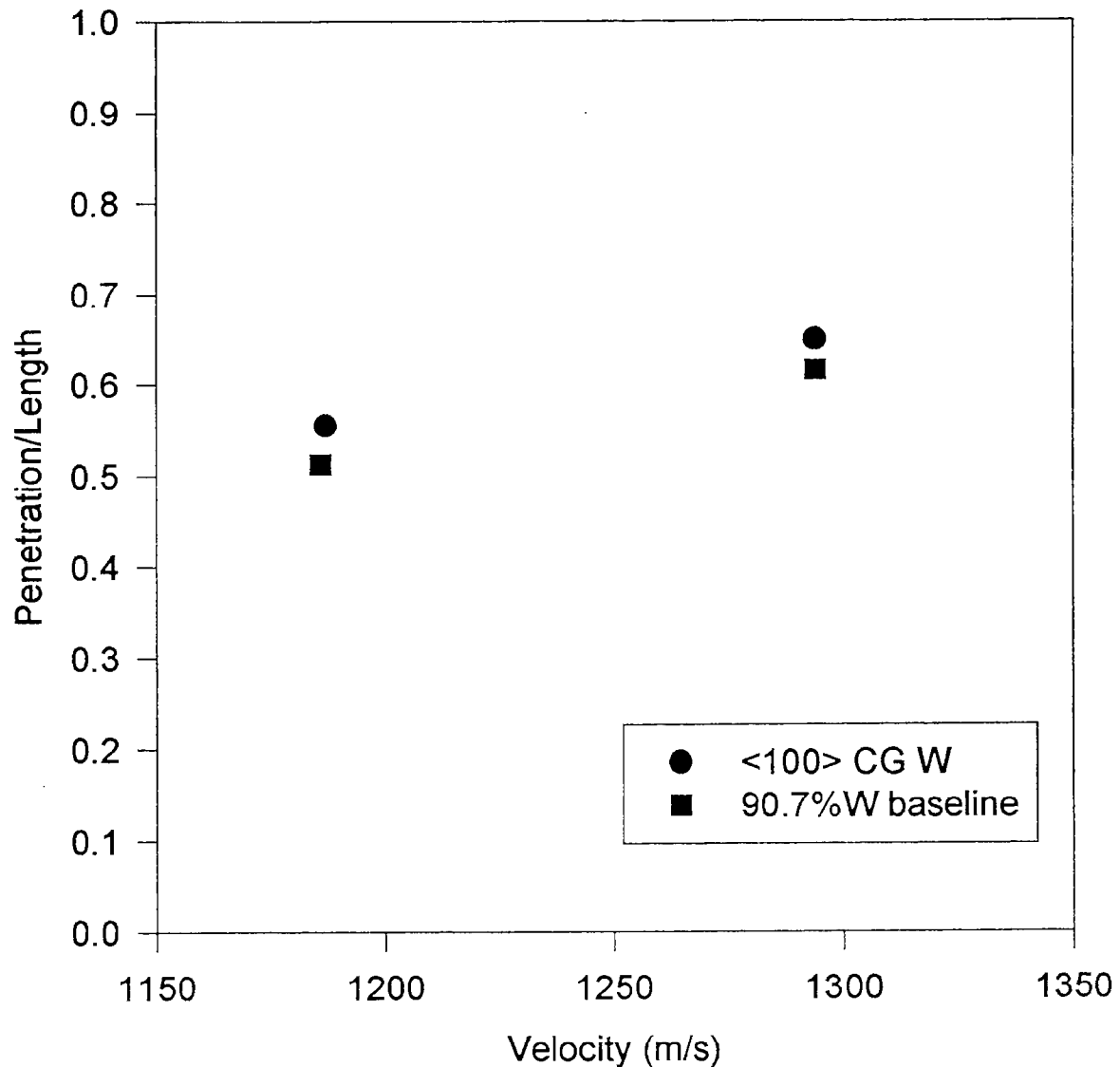
Figure 13. Quarter-Scale Ballistic Results.

these residual penetrators are compared to those of the residual penetrators recovered in the monocrystal tests by Bruchey, Horwath, and Kingman (1990).

As a baseline for comparison, the residual penetrators from tests of random-orientation, fine-grained tungsten (i.e., nonsag tungsten) were examined. The isotropic, fine-grained tungsten penetrators deform in an extremely stable manner (Gerlach 1986; Magness 1992). A large, mushroomed head forms on the penetrator as it is inverted at the penetrator-target interface (Figure 14a). There is a steady flow of material around the shoulder of the mushroomed head

17
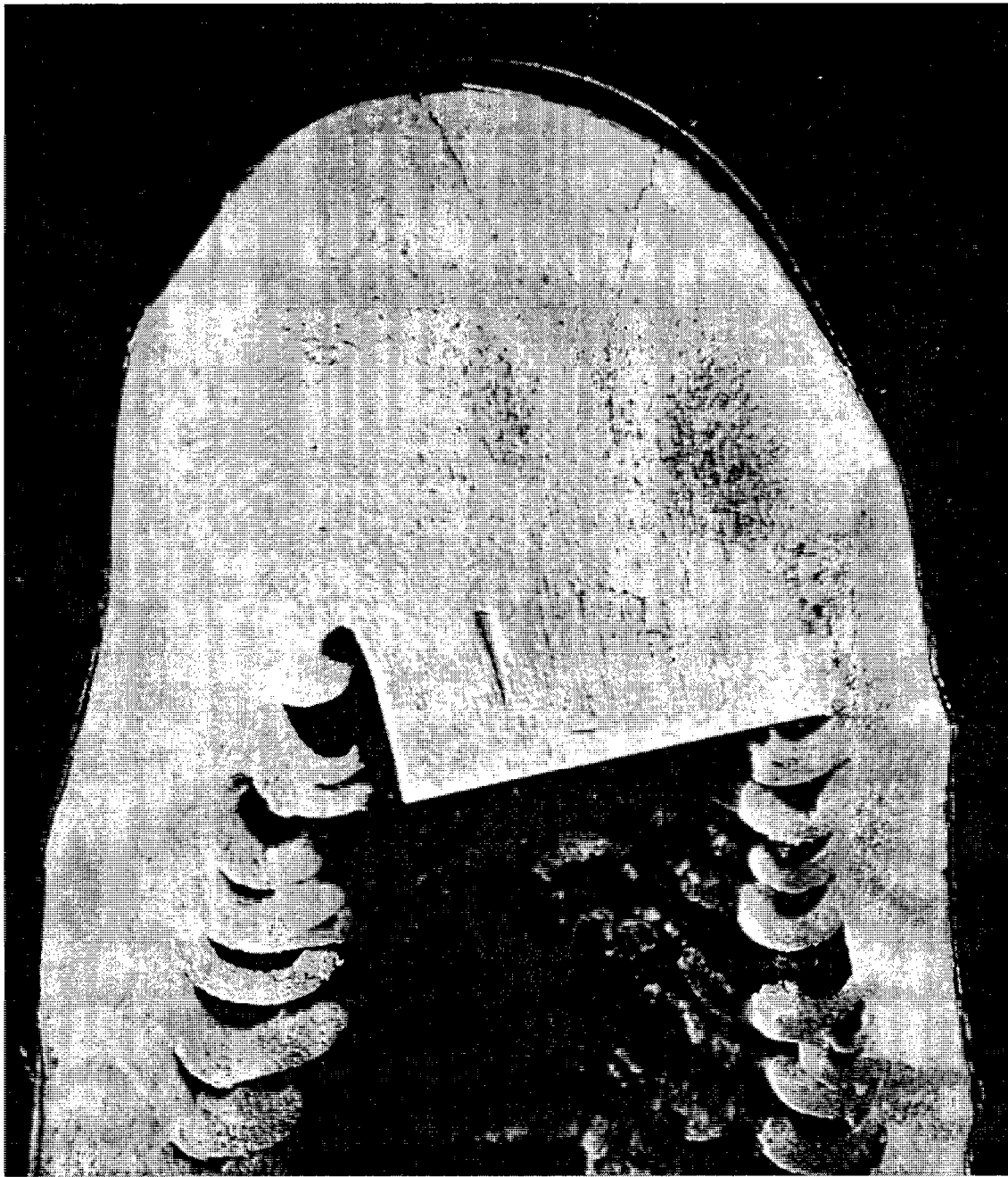
(a) Overview of Residual Penetrator.

Figure 14. Residual Polycrystalline Fine-Grained Tungsten Penetrator.
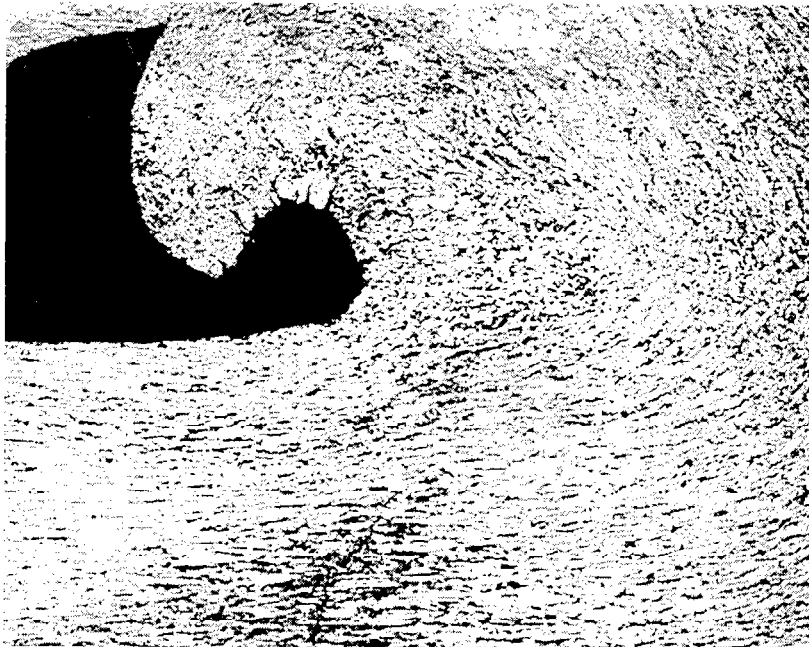
(b) Deformation About the Shoulder of Penetrator (37.5×).
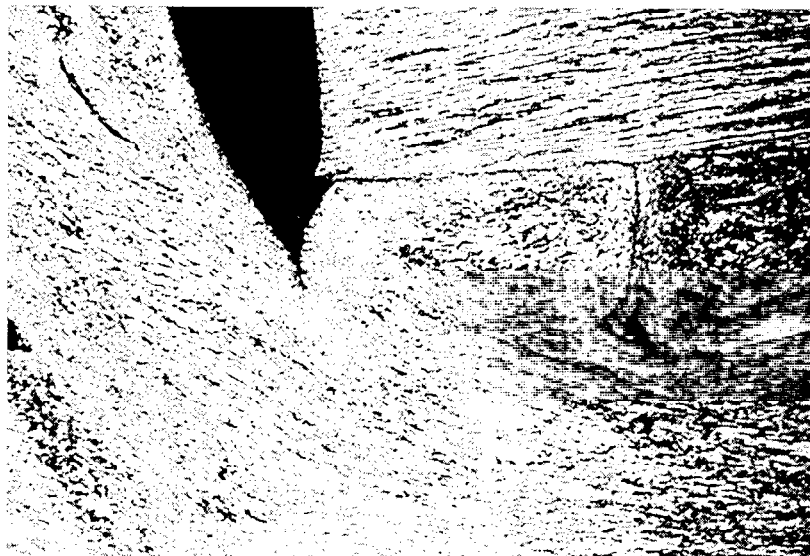
(c) Discarded Exfoliations (75×).

Figure 14. Residual Polycrystalline Fine-Grained Tungsten Penetrator (continued).

(Figure 14b), until the deformed material is eventually discarded in rather thick exfoliations from the shoulder and the periphery of the head (Figure 14c). The steady and stable flow of eroding penetrator materials results in a smooth-walled penetration cavity in the armor.

The optical micrographs of the residual [110]-oriented columnar-grained penetrators are shown in Figures 15a–e. The entire columnar-grained [110] residual penetrator was heavily deformed, with two sets of crisscrossing deformation bands throughout the interior of the residual penetrator stub (Figure 15b). At higher magnification, the bands in the rear of the penetrator appear to be a series of discontinuous lenticular shapes (Figure 15c).

The stable deformation of the [110]-oriented columnar-grained material produced a penetration cavity with very smooth walls. The columnar-grained material was clearly both heavily worked and extensively recrystallized in those regions of the residual mushroomed penetrator near the penetrator-target interface, such as the front of the mushroomed head and the previously discarded material, which now lined the penetration tunnel walls (Figure 15d). The overall deformation and discard of the exfoliations appeared to be quite ductile. The individual exfoliations (Figure 15e) were thinner than those discarded from the fine-grained, polycrystalline tungsten penetrators (Figures 14a and c).

An overall view of a residual [111]-oriented columnar-grained tungsten penetrator is shown in Figure 16a. Blocks of less deformed material appear to discard from the head of the penetrator along bands of heavily deformed material. This mix of heavily deformed and less deformed material forms the erosion products that line the penetration cavity (Figure 16b). An extensive and crisscrossing pattern of slip or deformation bands, with the less deformed regions in between, divides the entire interior of the residual projectile (Figure 16c). The material becomes more heavily worked, and the bands more closely spaced, in regions closer to the penetrator-target interface and the periphery of the head on the penetrator (Figure 16d). In both Figures 16d and e (a higher magnification examination of a region near the periphery of the mushroomed head), the deformation and recrystallization are extensive but uneven or inhomogeneous. This contrasts with the more continuous deformation seen for the [110]-oriented columnar tungsten (Figure 15d) and the equiaxed polycrystalline tungsten penetrator (Figure 14).

20

(a) Overview of Residual Penetrator (10×).

Figure 15. Residual [110]-Oriented Columnar-Grained Tungsten Penetrator.

21

(b) Two Sets of Deformation Bands (37.5×).

(c) Discontinuous Lenticular Microstructure Within Deformation Bands (150×).

Figure 15. Residual [110]-Oriented Columnar-Grained Tungsten Penetrator (continued).

22
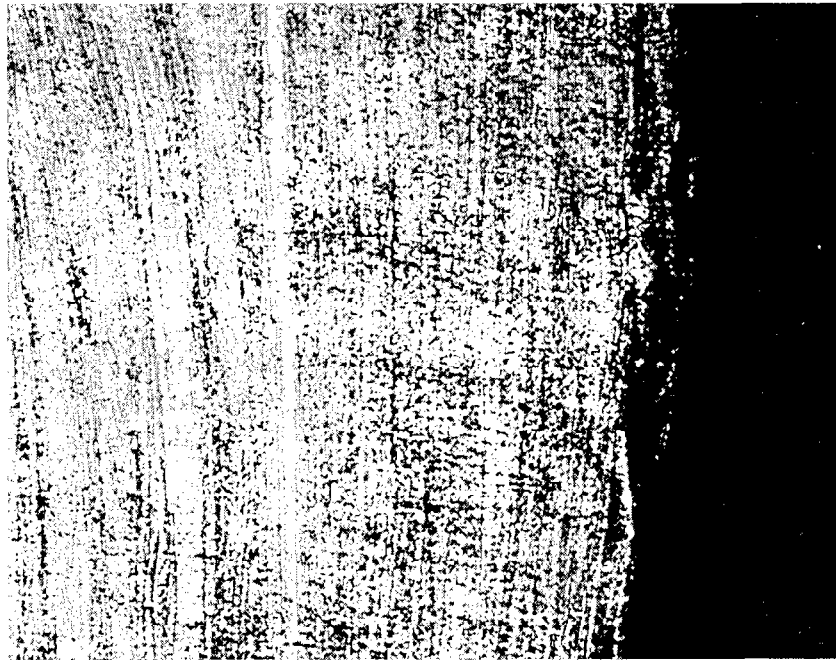
(d) Heavily Worked Tungsten Lining Penetration Cavity Walls (150×).
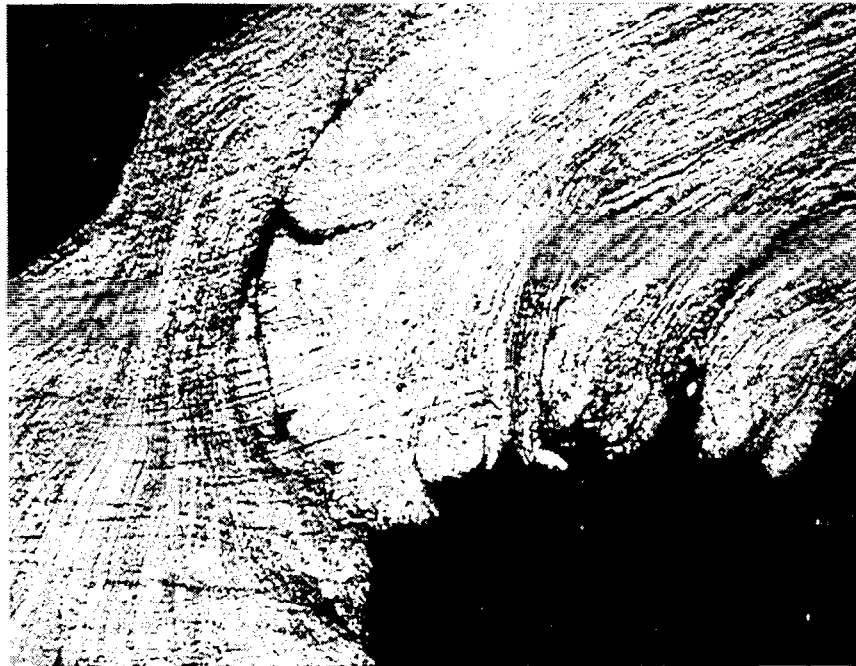
(e) Discarded Exfoliations (37.5×).

Figure 15. Residual [110]-Oriented Columnar-Grained Tungsten Penetrator (continued).

23

(a) Overview of Residual Penetrator (10×).

Figure 16. Residual [111]-Oriented Columnar-Grained Tungsten Penetrator.

24

(b) Heavily Deformed and Less Deformed Erosion Products Lining the Penetration Cavity (75×).

(c) Deformation Bands Dividing Interior (75×).

Figure 16. Residual [111]-Oriented Columnar-Grained Tungsten Penetrator (continued).

(d) Heavily Worked Tungsten Near Periphery of Head (75×).

(e) Extensive Deformation and Recrystallization (375×).

Figure 16. Residual [111]-Oriented Columnar-Grained Tungsten Penetrator (continued).

26

The residual penetrator recovered from a [100]-oriented columnar-grained penetrator test is shown in Figure 17a. A pattern of both curved and relatively straight slip or deformation bands cross one another throughout the entire residual penetrator. Near the rear of the penetrator, both sets of slip bands are relatively straight but one set is generally much wider than the other (Figure 17b). The blocks of material defined by these bands are sharply angular, in contrast to the rounded, eye-shaped regions outlined in the [111] columnar-grained penetrators. A substructure is apparent within both sets of bands at higher magnifications (Figures 17c and d). Nearer the periphery of the mushroomed penetrator's head, the deformation bands are curved and clearly recrystallized (Figure 17e). At the shoulder of the mushroomed penetrator (Figure 17f), the material is discarded along the slip or deformation bands. The discarded or exfoliated material lining the penetration cavity shows evidence of extensive plastic deformation and recrystallization (Figure 17g).

The substructures (Figures 17c and 17d) and lenticular shapes (Figure 15c) observed in the deformation bands found in all three orientations of residual columnar-grained penetrators suggest microbanding, or possibly twinning, deformations. To distinguish between these two possibilities will require detailed electron diffraction pattern analyses, due to the coincidence of twin reflections and matrix reflections for several common orientations in body-centered cubic (BCC) materials (Murr and Pappu 1996; Murr et al. 1996, 1997).

5. Discussion

5.1 Behavior and Performance of Tungsten Monocrystals. The major goal of this study was to see whether the distinct flow and failure behaviors and differing penetration performances, noted by Bruchey, Horwath, and Kingman (1990) for the tungsten monocrystal penetrators, would also be observed for columnar-grained tungsten penetrators having the same orientations.

The penetration data from the 1990 tests of [100]-, [110]-, and [111]-oriented monocrystals, and U-3/4% Ti and 93-weight-percent tungsten WHA penetrators, conducted at an impact velocity of 1,500 m/s, are summarized in Table 3. These results can be compared with those obtained in this
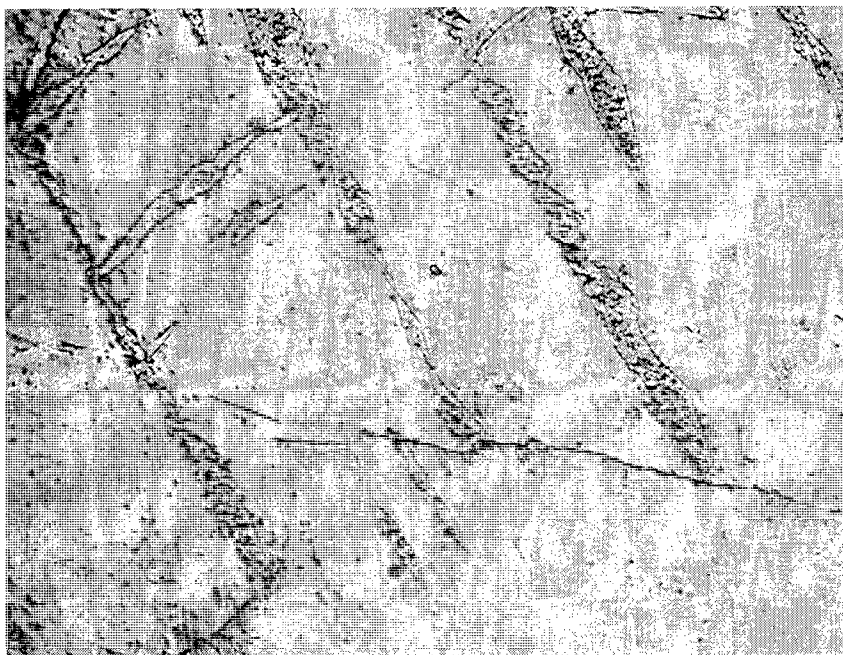
(a) Overview of Residual Penetrator (10×).

Figure 17. Residual [100]-Oriented Columnar-Grained Tungsten Penetrator.

28

(b) Intersecting Deformation or Slip Bands in Rear (75×).
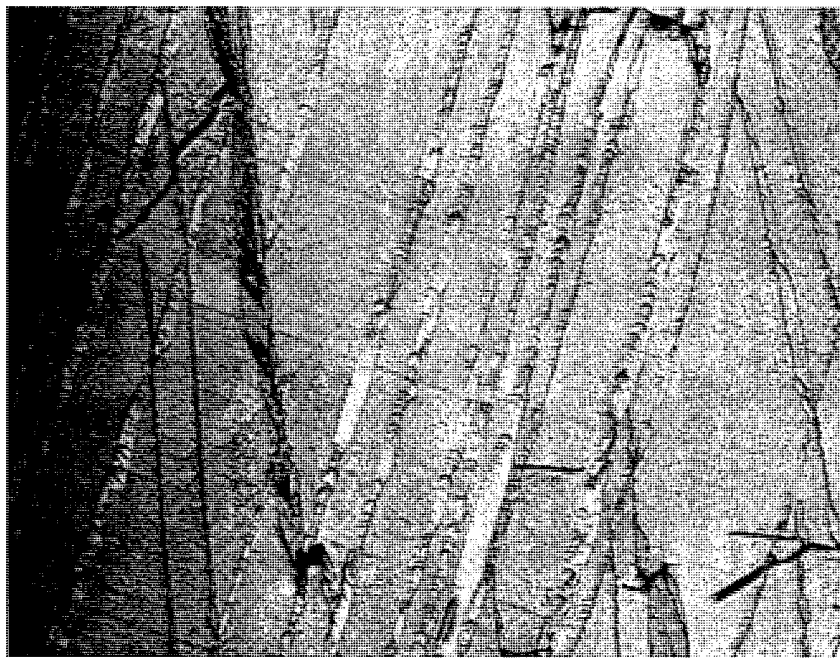
(c) Possible Twinning or Microbanding Within Deformation Bands (188×).

Figure 17. Residual [100]-Oriented Columnar-Grained Tungsten Penetrator (continued).

(d) Possible Twinning or Microbanding Within Deformation Bands (Murr and Pappu 1997).
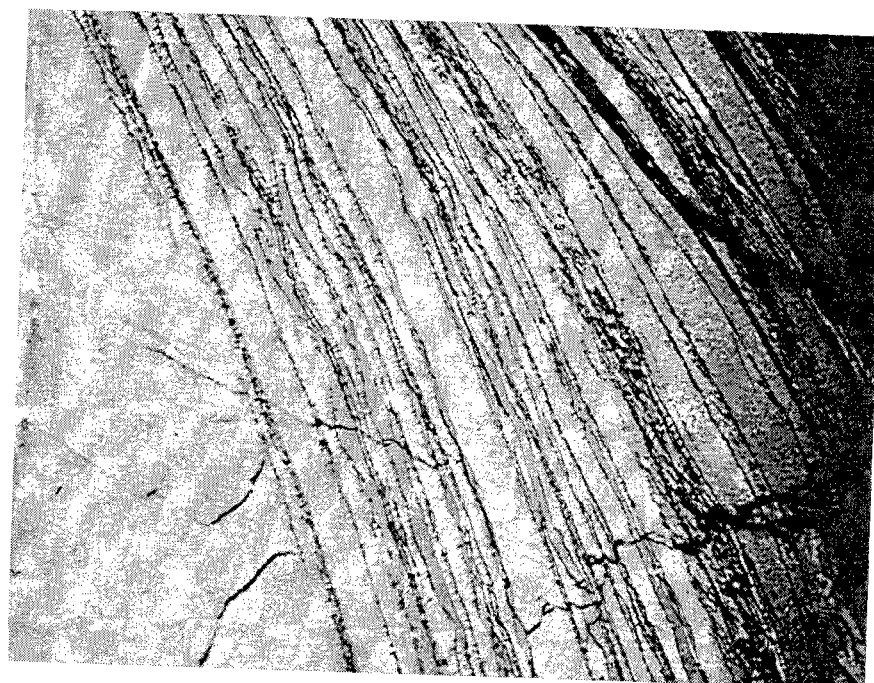
(e) Recrystallized Deformation Bands Near Periphery of Mushroomed Head (150×).

Figure 17. Residual [100]-Oriented Columnar-Grained Tungsten Penetrator (continued).

(f) Deformation at Shoulder of Penetrator (37.5×).

(g) Discarded Exfoliations (75×).

Figure 17. Residual [100]-Oriented Columnar-Grained Tungsten Penetrator (continued).

31

Table 3. Penetration Results for Tungsten Monocrystals.

Penetrator Material	Mass (g)	Length (mm)	Velocity Adjusted Penetration (mm)	P/L
93% W	75.5	106.6	89.7	0.84
93% W	74.5	112.9	93.5	0.83
[100]	74.2	102.5	99.8	0.97
[110]	73.7	102.5	83.0	0.81
[110]	73.6	102.5	88.0	0.86
[111]	74.2	102.5	89.9	0.88
[111]	73.7	102.5	90.3	0.88
U-3/4% Ti	74.0	104.4	99.0	0.95
U-3/4% Ti	74.0	104.4	99.4	0.95

NOTES: Tests conducted at 1,500 m/s by Bruchey, Horwath, and Kingman (1990).
W = Tungsten.

study, listed in Table 1. As noted earlier, the tungsten monocrystal penetrators delivered much greater differences in ballistic performances than the three orientations of columnar-grained materials. Also note that the [100] monocrystal penetrators delivered penetration performance roughly equivalent to that of the U-3/4% Ti penetrators, while the [100]-oriented columnar-grained penetrators offered only slightly greater penetration performance than the other orientations and fell far short of that of U-3/4% Ti penetrators.

Bruchey, Horwath, and Kingman (1990), Herring (1992), and Kingman and Herring (1995) examined the residual monocrystal penetrators in each orientation using optical metallography, TEM, and x-ray diffraction techniques. Macrographs of each of the residual penetrators, from Bruchey, Horwath, and Kingman (1990), are shown in Figures 18a–c. The distinct flow and failure behaviors exhibited by each orientation during the penetration process are apparent. Only optical metallographic examinations have been performed to date on the residual-oriented columnar-grained penetrators, but the comparisons of both sets of optical metallographic observations, in combination

(a) [110] Orientation (10×).

Figure 18. Monocrystal Penetrators (Bruchey, Horwath, and Kingman 1990).
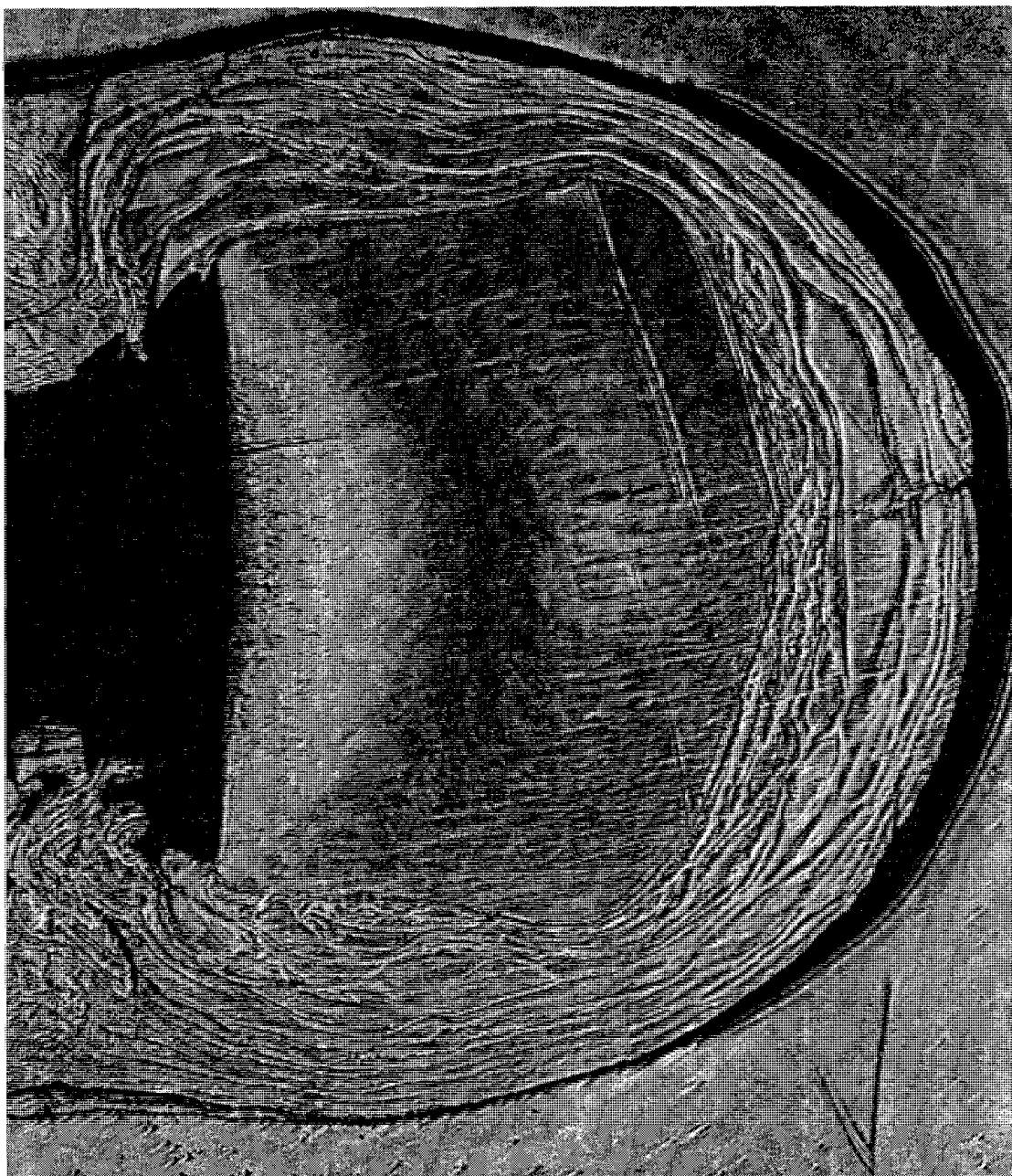
(b) [111] Orientation (10×).

Figure 18. Monocrystal Penetrators (Bruchey, Horwath, and Kingman 1990) (continued).

(c) [100] Orientation (10×).

Figure 18. Monocrystal Penetrators (Bruchey, Horwath, and Kingman 1990) (continued).

with the x-ray and TEM observations done in the monocrystal study, may provide some insights into the possible underlying flow and failure behaviors of the columnar-grained materials.

In BCC crystals such as tungsten, the slip directions are the close-packed, <111>, directions. A BCC crystal has no close-packed plane, however, and the slip planes are therefore not well defined. The {110}, {112}, and {123} planes, and perhaps others, may act as slip planes. The orientations of the slip planes and directions, relative to the penetrator axis and the forces applied to the head of the penetrator across the penetrator-target interface, will influence the deformation behaviors of both monocrystal and oriented columnar-grained penetrators.

5.2 Comparison of [110] Monocrystal and [110]-Oriented Columnar-Grained Penetrator. For a [110]-oriented BCC single crystal, only two of the <111> slip directions, at 35° to the penetrator axis, would be operable under a purely uniaxial load. The resolved shear stresses on these slip systems would be quite high. In static and dynamic uniaxial compression tests (Horwath and Ramesh 1994; Horwath 1994), a [110]-oriented single crystal exhibits a large load drop after yielding, followed by a period of easy glide deformation with a very low rate of work-hardening as the dislocations begin to tangle and interact. Of course, the loads applied to the head of the penetrator are more complex (triaxial). It would be an oversimplification in this case, and for penetrators with the other orientations as well, to expect their behavior to be based solely on the slip systems operable under uniaxial loads.

The overall deformation observed for the [110] monocrystal penetrator (Figure 18a) was stable, displacing a smooth-walled penetration cavity. However, the penetration cavity was also highly asymmetric, having an elliptical rather than circular cross section (Bruchey, Horwath, and Kingman 1990). Two intersecting sets of slip traces or deformation bands can be seen in the residual penetrator. The flow of material was very ductile, leaving a series of thin, ductile exfoliations lining the penetration cavity. Optical and x-ray examinations found evidence of extensive deformation, and nearly as extensive recrystallization, within the entire residual penetrator. Sharp x-ray diffraction patterns indicating equiaxed recrystallized grains, as well as broadened and textured rings indicating heavily worked material, were found (Kingman and Herring 1995). The TEM analysis

36

by Herring (1992) found moderately orderly arrays of straight screw dislocations, typical of those left behind by the passage of edge dislocations through the crystal. In all of these x-ray and TEM studies, no evidence of twinning was found for the [110] monocrystal penetrators or for the two other monocrystal orientations.

Under the metallographic examinations, the overall appearances of the residual monocrystalline [110] penetrators were very similar to those of the columnar-grained [110] penetrators (Figure 15a), and by far the most similar in the columnar-grained vs. monocrystal penetrator comparisons. In both the [110] monocrystal and the [110] columnar-grained projectiles, the entire residual penetrators had been heavily deformed, with two sets of slip or deformation bands crossing one another in the residual stubs (Figures 15b and 18a).

5.3 Comparison of [111] Monocrystal and [111]-Oriented Columnar-Grained Penetrator.
For the [111]-oriented monocrystal penetrator, three <111> slip directions, at 70.5° with respect to the penetrator axis, would be operable under a uniaxial load. The resolved shear stresses on these slip systems would be relatively low. The resultant yield strength of crystals of this orientation (Horwath and Ramesh 1994; Horwath 1994) is therefore relatively high. Dynamic compression tests again reveal a load drop after yielding. However, unlike the [110] monocrystals after the yield point drop, the deformation of the [111]-oriented monocrystals exhibited moderate work hardening.

The overall deformation observed for the [111] monocrystal penetrator appeared to be less stable than that of the [110] monocrystal. The slip bands appeared at angles more nearly perpendicular to the axis of the penetrator and were nearly absent within the interior of the residual penetrator. Like the [111] columnar-grained penetrators (Figure 16a), the [111] monocrystal penetrator discarded eroded material from its head in rounded or eye-shaped blocks of material (Figure 18b), along these slip bands. This chunky flow of material produced a waviness to the sides of the penetration cavity. Unlike the [111] columnar-grained penetrators, however, the crisscrossing pattern of slip or deformation bands alternating with the less deformed regions, did not divide the interior of the entire residual projectile. The rear of the penetrator was relatively undeformed and still a single crystal. The x-ray diffraction studies (Kingman and Herring 1995) confirmed these general impressions from

the optical metallography. The back-extruded [111] monocrystal material lining the walls of the penetration tunnel consisted largely of polycrystalline material with strong preferred orientations but also included some regions of bent or deformed single crystals (the rounded blocks). TEM analysis by Herring (1992) found orderly arrays of dislocations. The dislocations were wavy or bowed, indicating the motion of screw dislocations or dislocations with large screw components through the crystal.

5.4 Comparison of [100] Monocrystal and [100]-Oriented Columnar-Grained Penetrator.
For the [100] orientation, four <111> slip directions, at 54.7° with respect to the penetrator axis, would be operable under a purely uniaxial load. The corresponding resolved shear stresses on slip systems on {110} and {112} planes would be quite large. In quasi-static uniaxial tests, the yield strength is therefore relatively low. The rate of work hardening is quite high, however, due to the interactions of the large number of dislocations on the multiple, nearly equally favored slip systems. This behavior was observed in dynamic compression testing (Horwath and Ramesh 1994; Horwath 1994). The [100] uniaxial compression specimens exhibited a low yield strength but a high rate of work hardening. Unlike [110] and [111] compression specimens, no large-scale slip traces were evident on the surfaces of the [100] dynamic compression specimens after the tests. However, cracks appeared on {100} planes in the specimens. It is likely that these were nucleated by a dislocation reaction proposed by Cottrell (1958), in which intersections of two partial dislocations, 1/2 [111] and 1/2 [111], form sessile [001] dislocations. The buildup of these sessile dislocations would initiate the cleavage cracks or failures.

The flow and failure behavior of the [100] monocrystal as a penetrator (Figure 18c), observed by Bruchey, Horwath, and Kingman (1990), was very different from the behaviors observed for the other two monocrystal orientations. Except in small regions at the shoulders of the mushroomed head, slip or deformation bands are nearly absent in the residual penetrator and the erosion products. This is consistent with the lack of slip traces noted in the dynamic compression specimens. The overall deformation of the [100] monocrystal appears to be a combination of lattice bending and rigid rotation acting to invert and discard penetrator material from the head of the projectile. Cleavage cracks, aligned parallel and perpendicular to the penetrator axis in the base of the residual

penetrator, and curving and opening radially in the inverting material, accommodate the required reorientation of blocks of crystal. The x-ray diffraction studies (Kingman and Herring 1995) confirmed this description. With the exception of the banded regions near the shoulder of the penetrator, the diffraction patterns remained sharp, without asterism, throughout the entire residual penetrator, but showed discrete changes in orientation (rotating) to follow the flow of penetrator material. TEM studies (Herring 1992) of the blocks of material revealed disorderly and tangled arrays of wavy dislocations, produced by the motion of screw dislocations or dislocations with large screw components. Consistent with the optical metallography of the [100] specimens, the disorderly dislocation arrays indicate that little recrystallization had occurred.

The deformation and failure behaviors exhibited by the residual [100]-oriented columnar-grained penetrator (Figure 17a) and the [100] monocrystal penetrator (Figure 18c) bore little resemblance to each other. Noticeably absent in the [100] columnar-grained penetrators were the cleavage cracks that were parallel and perpendicular to the penetrator axis for the [100] orientation monocrystal penetrators. Instead, there was a pattern of both curved and relatively straight slip or deformation bands (which were largely absent in the [100] monocrystal) crisscrossing one another throughout the entire residual penetrator. In many regions, especially near the periphery of the [100] columnar-grained penetrator's mushroomed head, the deformation bands are clearly recrystallized (Figure 17e), while very little recrystallization was seen in any area of the [100] monocrystal penetrator. The deformation of the columnar-grained tungsten at the shoulder of the mushroomed penetrator (Figure 17f) also clearly differs from that of [100] monocrystals (Figure 19); the pattern of lattice rotation and opening cleavage planes in the monocrystal has been replaced by a discard of material along slip or deformation bands. The discarded or exfoliated [100] columnar-grained material lining the penetration cavity shows evidence of extensive plastic deformation and recrystallization, but, again, no pattern of cleavage failures (Figure 13g).

5.5 Overview of Monocrystal and Columnar-Grained Penetrator Behaviors and Performances. In the optical metallographic examinations, the appearances of [110] monocrystal penetrators and erosion products bore a strong resemblance to that of [110] columnar-grained penetrator and erosion products. For the other two orientations, however, there were striking
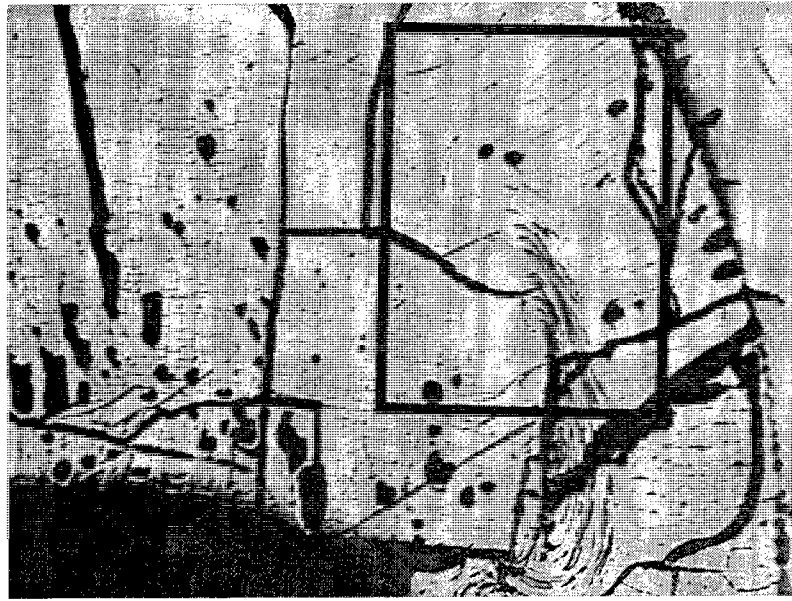
Figure 19. Deformation at the Shoulder of a [100]-Oriented Monocrystal Penetrator.

differences. For the [111] orientation, the most notable differences were in the deformations of the residual penetrator stubs, relatively undeformed in the [111] monocrystal penetrators but crisscrossed by a pattern of deformation bands in the [111] columnar-grained penetrators. How the grain and subgrain misorientations and the presence of the grain and subgrain boundaries might have caused these contrasting behaviors cannot be determined from these optical metallographic comparisons. X-ray and TEM studies in the future may help answer some of these questions. The differences between [100] monocrystal penetrator and [100] columnar-grained penetrator flow and failure behaviors were even more striking. The most significant differences were: (1) deformation bands were present in the residual penetrator and the discarded erosion products lining the penetration cavity of the [100] columnar-grained penetrator but not the [100] monocrystal and (2) the cleavage failure mechanism operated in the [100] monocrystal penetrators but not in the [100] columnar-grained penetrators. The presence of slightly misoriented grains and grain and subgrain boundaries appear to prevent the formation of cleavage cracks via the buildup of sessile dislocations (Cottrell 1958) within the columnar-grained material. It may be that, under these conditions, other dislocation mechanisms such as cross slip are facilitated. Again, no determination is possible from these optical metallographs, but future x-ray and TEM examinations may answer some of these questions.

40

The pattern that emerges from these comparisons is that each of the orientations of monocrystal penetrators exhibited very distinct deformation and failure behaviors and each delivered significantly different performances as penetrators (Bruchey, Horwath, and Kingman 1990). Both the erosion products and residual penetrator stubs of the [110] monocrystal penetrators underwent extensive deformation and recrystallization. This orientation offered the poorest performance. For the [111]-oriented monocrystal, the deformation and recrystallization of erosion products was less uniformly distributed and less extensive within the residual penetrator stub. This orientation offered intermediate penetration performance. For the [100]-oriented monocrystal, the deformation was dominated by cleavage and lattice rotation. Little deformation banding or recrystallization was apparent in either the erosion products or the residual penetrator stub. This orientation offered the best performance, approximately equaling that of U-3/4% Ti penetrators. In these follow-on tests of oriented columnar-grained tungsten penetrators, the behaviors were much less distinct. Deformation banding and recrystallization were observed in both the erosion products and the residual penetrator stubs for all three orientations. Although the relative ranking of the penetration performances was still the same as for the monocrystal penetrators, the differences between their performances were quite small.

6. Conclusions

The flow and failure behavior of a penetrator material influences the proportion of the penetrator's KE expended as work to displace and widen a penetration cavity in the armor (Magness and Farrand 1990). Tungsten single crystals with [100], [110], and [111] orientations exhibited very distinct deformation, flow, and failure behaviors during their penetration of armor (Bruchey, Horwath, and Kingman 1990). Correspondingly, there were significant differences in the final penetration depths achieved by penetrators of each orientation.

The rankings of the ballistic performances of [100]-, [110]-, and [111]-oriented columnar-grained penetrators were the same as for the monocrystal penetrators; however, the range of performances was much narrower. The performances of the [100]-oriented columnar-grained tungsten penetrators

were only slightly superior to that of random-oriented, fine-grained pure tungsten penetrators and far short of the nearly U-3/4% Ti equivalent performance delivered by the [100] monocrystal orientation. The differences in the flow and failure behaviors among the columnar-grained tungsten polycrystals were also less distinct. Optical metallographic examinations of the residual penetrators recovered from the tests showed evidence of the activity of multiple slip systems and regions of extensive plastic deformation and recrystallization for all three orientations.

It is difficult to draw too many conclusions about the performance of columnar-grained tungsten penetrator materials based solely on the optical metallographic examinations carried out to date. X-ray and TEM studies now underway may provide additional insights to their behaviors. It is clear, however, that the misorientations of the individual columnar grains, with respect to the penetrator axis and each other, influenced the flow and failure behaviors of these materials and reduced the differences between the performances of the penetrators having three different crystallographic orientations. These results suggest that any attempts to impart some of the penetration advantages of the [100] monocrystal's flow and failure behavior to a polycrystalline tungsten aggregate (by mechanically working the material to develop a [100] texture) or to a tungsten-based metal matrix composite (by orienting the tungsten phase) will probably not be successful.

7. References

Bruchey, W., E. Horwath, and P. Kingman. "Effect of Crystallographic Orientation on the Performance of Single Crystal Tungsten Sub-Scale Penetrators." BRL-MR-941, U.S. Army Ballistic Research Laboratory, Aberdeen Proving Ground, MD, April 1990.

Bruchey, W., E. Horwath, and P. Kingman. "Orientation Dependence of Deformation and Penetration Behavior of Tungsten Single Crystal Rods." *Tungsten and Tungsten Alloys - Recent Advances*, A. Crowson and E. Chen (editors), p. 121, 1991.

Cottrell, A. H. "Theory of Brittle Fracture in Steel and Similar Metals." *Trans. Met. Soc. of AIME*, p. 192, 1958.

Gerlach, U. "Microstructural Analysis of Residual Penetrators - A New Method to Explain Penetration Mechanisms." *Met. Trans.*, vol. 17A, pp. 435–442, 1986.

Horwath, E. J. "The High Strain Rate Deformation of Tungsten Single Crystals." ARL-TR-620, U.S. Army Research Laboratory, Aberdeen Proving Ground, MD, November 1994.

Horwath, E. J., and K. T. Ramesh. "The High Strain Rate Deformation of Tungsten Single Crystals." *Tungsten and Refractory Metals 2*, A. Bose and R. Dowding (editors), 1994.

Herring, R. A. "Determination of Operable Deformation Mechanisms During Ballistic Impact in Tungsten Single Crystals, Using Transmission Electron Microscopy." BRL-TR-3385, U.S. Army Ballistic Research Laboratory, Aberdeen Proving Ground, MD, August 1992.

Kim, M. R., R. W. Smith, and D. Kapoor. "Vacuum Plasma Spray Deposition of Tungsten Base Functionally Gradient Composites." *Thermal Spray: Practical Solutions for Engineering Problems*, C. C. Berndt (editor), pp. 7–12, 1996.

Kingman, P., and R. Herring. "Ballistic Penetration Phenomenology of High Symmetry Single Crystals." ARL-TR-700, U.S. Army Research Laboratory, Aberdeen Proving Ground, MD, February 1995.

Leonard, W., L. Magness, R. Dowding, J. Trogolo, M. Chung, and D. Kapoor. "Ballistic Performance of Oriented Columnar-Grained Tungsten Polycrystals." *Tungsten and Refractory Metals 3*, A. Bose and R. Dowding (editors), 1995.

Leonard, W., L. Magness, and D. Kapoor. "Ballistic Evaluation of Thermo-Mechanically Processed Tungsten Heavy Alloys." BRL-TR-3326, U.S. Army Ballistic Research Laboratory, Aberdeen Proving Ground, MD, April 1992.

Magness, L. "A Phenomenological Investigaation of the Behavior of High-Density Materials Under the High-Pressure, High-Strain-Rate Loading Environment of Ballistic Impact." Ph. D. Dissertation, Johns Hopkins University, 1992.

Magness, L., and T. Farrand. "Deformation Behavior and Its Relationship to the Penetration Performance of High Density KE Penetrator Materials." *Proceedings From the 1990 Army Science Conference,* Durham, NC, May 1990.

Murr, L., C-S. Niou, E. Ferreyra, S. Pappu, C. Kennedy, S. A. Quinones, J. M. Romero, and J. Maldonaldo. "Multi-Dimensional Microanalysis in materials Characterization: Some Case Examples." *Developments in Materials Characterization Technologies,* G. Vandervolt and J. Friel (editors), pp. 1–13, ASM International, Materials Park, OH, 1996.

Murr, L., and S. Pappu. Private communication. University of Texas, El Paso, October 1997.

Murr, L., J. M. Rivas, E. Ferreyra, and J. C. Sanchez. "A Comparison of Deformation Twins and Deformation-Induced Microbands in Copper." *Microstructural Sciences Vol. 24, Understanding Microstructure: Key to Advance in Materials,* edited by M. G. Burke, E. Clark, and E. J. Palmiere (editors), pp. 121–132, ASM International, Materials Park, OH, 1997.

Trogolo, J. "Crystallographic Analysis of <001>, <011>, and <111> Tungsten Crystals." Contract No. W71B7J-95-M-S109, Niche Microstructural Corporation, April 1995.

Appendix:

Summary of Individual Shot Data

INTENTIONALLY LEFT BLANK.

Table A-1. Conventional Tungsten Penetrator Data Summary

Shot No.	Penetrator Material (% of Tungsten)	Length (mm)	Dia. (mm)	Mass (g)	Pitch$_{pen}$ (°)	Target Material	Length (mm)	Dia. (mm)	Hardness (BHN)	Pitch (°)	Yaw (°)	Vel. (m/s)	Hit Location (mm)	Adjusted Penetration (mm)
4	93	50.39	3.91	10.3	0	Mild Steel	38.12	46.81	143	NM[b]	NM	1,003	NM	26.0
5	93	50.44	3.94	10.3	0.21	Mild Steel	37.99	46.93	143	NM	NM	1,004	20	27.0
4405	97	50.68	3.77	10.77	0.35	Mild Steel	63.50	46.93	131	0	0	1,025	20	27.7
4407	97	50.70	3.88	11.14	1.52	Mild Steel	63.50	nr[a]	131	0	0	998	20	27.7
4409	97	50.80	3.86	10.99	1.0	Mild Steel	63.50	nr[a]	131	0	0	1,006	ok	28.8

[a] nr = not recorded.
[b] NM = not measured.

Table A-2. Nonsag Tungsten Penetrator Data Summary

Shot No.	Penetrator Material	Length (mm)	Dia. (mm)	Mass (g)	Pitch$_{pen}$ (°)	Target Material	Length (mm)	Dia. (mm)	Hardness (BHN)	Pitch (°)	Yaw (°)	Vel. (m/s)	Hit Location (mm)	Adjusted Penetration (mm)
70	Nonsag Tungsten	50.80	3.84	11.38	Lost	Mild Steel	50.8	46.9	149	Lost	Lost	Lost	20	27.0

47

Table A-3. <100>-Oriented Columnar-Grained Tungsten Penetrator Data Summary

Shot No.	Penetrator Material	Length (mm)	Dia. (mm)	Mass (g)	Pitch$_{pen}$ (°)	Target Material	Length (mm)	Dia. (mm)	Hardness (BHN)	Pitch (°)	Yaw (°)	Vel. (m/s)	Hit Location (mm)	Adjusted Penetration (mm)
133	<100>	52.07	3.76	11.34	0.21	Mild Steel	50.80	46.98	149	0.75	−0.50	1,006	19.5	30.3
160	<100>	52.28	3.71	11.46	0.42	Mild Steel	50.67	46.96	156	−1.0	−0.75	1,011	20	31.2
170	<100>	52.02	3.73	11.39	0	Mild Steel	50.80	46.93	149	−2.5	−2.5	1,005	18.8	29.3
191	<100>	50.86	3.73	10.82	0	Mild Steel	50.83	46.86	149	−1.0	1.0	1,023	19.8	28.3

48

Table A-4. <110>-Oriented Columnar-Grained Tungsten Penetrator Data Summary

Shot No.	Penetrator Material	Length (mm)	Dia. (mm)	Mass (g)	Pitch$_{pen}$ (°)	Target Material	Length (mm)	Dia. (mm)	Hardness (BHN)	Pitch (°)	Yaw (°)	Vel. (m/s)	Hit Location (mm)	Adjusted Penetration (mm)
136	<110>	50.80	3.73	10.96	0.42	Mild Steel	50.80	46.94	149	1.0	−1.75	1,017	18.3	24.5
153	<110>	50.74	3.82	11.35	0.42	Mild Steel	50.76	46.84	126	0.5	0	1,018	21.34	26.2

Table A-5. <111>-Oriented Columnar-Grained Tungsten Penetrator Data Summary

Shot No.	Penetrator Material	Length (mm)	Dia. (mm)	Mass (g)	Pitch$_{pen}$ (°)	Target Material	Length (mm)	Dia. (mm)	Hardness (BHN)	Pitch (°)	Yaw (°)	Vel. (m/s)	Hit Location (mm)	Adjusted Penetration (mm)
134	<111>	50.74	3.81	11.28	0.63	Mild Steel	50.79	46.98	156	1.25	−0.75	1,016	21.1	25.0
154	<111>	50.67	3.81	11.46	0.42	Mild Steel	50.82	46.90	131	0	1.25	1,010	20.0	29.8

Table A-6. U-3/4% Ti Penetrator Data Summary

Shot No.	Penetrator Material	Length (mm)	Dia. (mm)	Mass (g)	Pitch$_{pen}$ (°)	Target Material	Length (mm)	Dia. (mm)	Hardness (BHN)	Pitch (°)	Yaw (°)	Vel. (m/s)	Hit Location (mm)	Adjusted Penetration (mm)
4403	U-3/4% Ti	50.80	3.89	10.93	2.5	Mild Steel	63.50	46.91	nr[a]	0	0	1,016	ok	38.9
4406	U-3/4% Ti	50.55	3.86	10.9	2.3	Mild Steel	63.50	46.91	nr	0	0	1,029	ok	39.9
4412	U- 3/4% Ti	50.80	3.91	11.0	2.37	Mild Steel	63.68	46.91	nr	0	0	1,026	ok	40.6

[a] nr = not recorded.

INTENTIONALLY LEFT BLANK.

NO. OF COPIES	ORGANIZATION	NO. OF COPIES	ORGANIZATION
4	CDR ARDEC D KAPOOR M CHUNG S CYTRON K WILLISON PICATINNY ARSENAL NJ 07806-5000	2	SW RSCH INST C ANDERSON J LANKFORD PO DRAWER 28510 6220 CULEBRA RD SAN ANTONIO TX 78228-0510
2	DIR ARO A CROWSON E CHEN PO BOX 12211 RESEARCH TRIANGLE PARK NC 27709-2211	2	UNIV OF CA SAN DIEGO DEPT OF APLD MECH AND ENG SCIENCE M MEYERS S NEMAT-NASSER LA JOLLA CA 92093
3	DIR LANL ATAC MS F681 B HOGAN P DUNN R GREY PO BOX 1663 LOS ALAMOS NM 87545	1	UNIV OF MO-ROLLA DEPT OF MECH ENG R BATRA ROLLA MO 65401
		1	AEROJET M MABRY BOX 13222 SACRAMENTO CA 95813
2	INST FOR ADVNCD TECH UNIV OF TX AUSTIN S BLESS R SUBRAMANIAN 4030-2 W BRAKER LN AUSTIN TX 78759	3	ALLIANT TECHSYS S NELSON M JONES T STEIGAUF 2225 NORTHLAND DR BROOKLYN PARK MN 55428
1	JOHNS HOPKINS UNIV DEPT OF MECHANICAL ENG K RAMESH 3400 N CHARLES ST BALTIMORE MD 21218	1	CERACON INC R RAMAN 1401 N MARKET BLVD STE 9 SACRAMENTO CA 95834
1	PENN STATE UNIV DEPT OF ENG SCNC AND MECH R GERMAN 227 HAMMOND BLDG UNIVERSITY PARK PA 16802-1401	1	CONCURRENT TECH INC T MCCABE 1450 SCALP AVE JOHNSTOWN PA 15904
1	RSRCH TRNGL INST J POSTHILL PO BOX 12194 RESEARCH TRIANGLE PARK NC 22209-2154	1	PARATECH CORP A BOSE 2221 PINE VIEW WAY PETALUMA CA 94952

NO. OF
COPIES   ORGANIZATION

1   ULTRAMET INC
        J STIGLICH
        12173 MONTAGUE ST
        TACOMA CA 91331

        ABERDEEN PROVING GROUND

31   DIR, ARL
        AMSRL WM T,
            W MORRISON
            T WRIGHT
        AMSRL WM TA,
            S BILYK
            W BRUCHEY
            M BURKINS
            E HORWATH
            E RAPACKI
        AMSRL WM TC,
            R COATES
            W DE ROSSET
            E KENNEDY
            W LEONARD (4 CPS)
            L MAGNESS
            R MUDD
            G SILSBY
            R SUMMERS
            W WALTERS
        AMSRL WM TD,
            G BOYCE
            S CHOU
            A DIETRICH
            T FARRAND
            K FRANK
            P KINGMAN
            M RAFTENBERG
            S SHOFIELD
            T WEERASOORIYA
        AMSRL WM TE,
            L KECSKES
        AMSRL WM BE,
            K CHO
            R DOWDING

INTENTIONALLY LEFT BLANK.

REPORT DOCUMENTATION PAGE

Public reporting burden for this collection of information is estimated to average 1 hour per response, including the time for reviewing instructions, searching existing data sources, gathering and maintaining the data needed, and completing and reviewing the collection of information. Send comments regarding this burden estimate or any other aspect of this collection of information, including suggestions for reducing this burden, to Washington Headquarters Services, Directorate for Information Operations and Reports, 1215 Jefferson Davis Highway, Suite 1204, Arlington, VA 22202-4302, and to the Office of Management and Budget, Paperwork Reduction Project(0704-0188), Washington, DC 20503.

1. AGENCY USE ONLY *(Leave blank)*	2. REPORT DATE	3. REPORT TYPE AND DATES COVERED
	May 1998	Final, January 1995 - November 1996

4. TITLE AND SUBTITLE

The Performance and Deformation Behavior of Oriented Columnar-Grained Tungsten Polycrystalline Penetrators

5. FUNDING NUMBERS

68T8G8

6. AUTHOR(S)

Lee S. Magness and Wendy A. Leonard, Deepak Kapoor,* Moon Chung,* and Jeffrey Trogolo**

7. PERFORMING ORGANIZATION NAME(S) AND ADDRESS(ES)

U.S. Army Research Laboratory
ATTN: AMSRL-WM-TC
Aberdeen Proving Ground, MD 21005-5066

8. PERFORMING ORGANIZATION REPORT NUMBER

ARL-TR-1666

9. SPONSORING/MONITORING AGENCY NAMES(S) AND ADDRESS(ES)

10. SPONSORING/MONITORING AGENCY REPORT NUMBER

11. SUPPLEMENTARY NOTES

*U.S. Army Armament Research, Development, and Engineering Center
**Niche Microstructural Corporation

12a. DISTRIBUTION/AVAILABILITY STATEMENT

Approved for public release; distribution is unlimited.

12b. DISTRIBUTION CODE

13. ABSTRACT *(Maximum 200 words)*

The flow and failure of monocrystalline tungsten penetrators, during the penetration of armor targets, has been shown to be anisotropic. The penetration performances of the single-crystal penetrators were found to be a function of the crystallographic orientation of the penetrator axis. The performance of the [100]-oriented tungsten penetrators was roughly equivalent to that of depleted uranium penetrators.

In this series of ballistic experiments, the performance and deformation behaviors of polycrystalline tungsten penetrators having oriented columnar grains in [100], [110], or [111] directions were examined.

14. SUBJECT TERMS

tungsten, columnar grains, monocrystal, penetration

15. NUMBER OF PAGES

60

16. PRICE CODE

17. SECURITY CLASSIFICATION OF REPORT	18. SECURITY CLASSIFICATION OF THIS PAGE	19. SECURITY CLASSIFICATION OF ABSTRACT	20. LIMITATION OF ABSTRACT
UNCLASSIFIED	UNCLASSIFIED	UNCLASSIFIED	UL

NSN 7540-01-280-5500

Standard Form 298 (Rev. 2-89)
Prescribed by ANSI Std. 239-18   298-102

INTENTIONALLY LEFT BLANK.